AAAS
Research
Volume 2019, Article ID 2763704, 10 pages
https://doi.org/10.34133/2019/2763704

Research Article

Confined van der Waals Epitaxial Growth of Two-Dimensional Large Single-Crystal In_2Se_3 for Flexible Broadband Photodetectors

Lei Tang[1], Changjiu Teng[1], Yuting Luo[1], Usman Khan[1], Haiyang Pan[2], Zhengyang Cai[1], Yue Zhao[2,3], Bilu Liu[1,*], and Hui-Ming Cheng[1,4,*]

[1] *Shenzhen Geim Graphene Center, Tsinghua-Berkeley Shenzhen Institute, Tsinghua University, Shenzhen 518055, China*
[2] *Shenzhen Institute for Quantum Science and Engineering and Department of Physics, Southern University of Science and Technology, Shenzhen 518055, China*
[3] *Shenzhen Key Laboratory of Quantum Science and Engineering, Shenzhen 518055, China*
[4] *Shenyang National Laboratory for Materials Sciences, Institute of Metal Research, Chinese Academy of Sciences, Shenyang 110016, China*

* Correspondence should be addressed to Bilu Liu; bilu.liu@sz.tsinghua.edu.cn and Hui-Ming Cheng; hmcheng@sz.tsinghua.edu.cn

Received 10 October 2018; Accepted 18 January 2019; Published 19 March 2019

The controllable growth of two-dimensional (2D) semiconductors with large domain sizes and high quality is much needed in order to reduce the detrimental effect of grain boundaries on device performance but has proven to be challenging. Here, we analyze the precursor concentration on the substrate surface which significantly influences nucleation density in a vapor deposition growth process and design a confined micro-reactor to grow 2D In_2Se_3 with large domain sizes and high quality. The uniqueness of this confined micro-reactor is that its size is ~10^2-10^3 times smaller than that of a conventional reactor. Such a remarkably small reactor causes a very low precursor concentration on the substrate surface, which reduces nucleation density and leads to the growth of 2D In_2Se_3 grains with sizes larger than 200 μm. Our experimental results show large domain sizes of the 2D In_2Se_3 with high crystallinity. The flexible broadband photodetectors based on the as-grown In_2Se_3 show rise and decay times of 140 ms and 25 ms, efficient response (5.6 A/W), excellent detectivity (7×10^{10} Jones), high external quantum efficiency (251%), good flexibility, and high stability. This study, in principle, provides an effective strategy for the controllable growth of high quality 2D materials with few grain boundaries.

1. Introduction

Two-dimensional (2D) materials have been considered promising candidates for miniaturized and high-performance electronic and optoelectronic devices due to their atomically flat and ultrathin nature and their lack of dangling bonds. Grain boundaries and defects in 2D materials can reduce charge transport, [1] mechanical, [2–4] and thermal properties [5]. Therefore, the controllable growth of 2D materials with large domain sizes and high quality with few grain boundaries and defects is important in order to achieve good device performance. To this end, different vapor deposition methods have been developed to grow 2D materials with large domain sizes, such as epitaxial growth on special substrates (e.g., sapphire [6] or mica [7, 8]), reducing nucleation density by locally feeding the precursors [9, 10], and passivating active sites during growth [11]. As summarized in Figure 1(a), the current domain sizes of semi-metallic graphene range from micrometers to meters [9, 12, 13], while semiconducting transition metal dichalcogenides (TMDCs) [14–16] and insulating hexagonal boron nitride (h-BN) have sizes up to hundreds of micrometers or larger [17–19]. Recently, another group of 2D materials with the structure A_2B_3, where A is a group III element and B is a group VI element, such as indium selenide (In_2Se_3, its structure is shown in Figure S1), has attracted increasing interest. First, In_2Se_3 has a direct bandgap of 1.36 eV [20], which is close to that of silicon (1.10 eV). Second, although some monolayer TMDCs like $MoTe_2$ also have a direct bandgap of 1.10 eV, they become indirect bandgap

materials as the number of layers increases [21], while In_2Se_3 is a direct bandgap material regardless of its thickness [22, 23]. Third, unlike black phosphorus which is also a direct bandgap 2D material, thin In_2Se_3 flakes are very stable in air, which is very important for practical applications. Recently, there has been pioneering work on the use of 2D In_2Se_3 in piezoelectronics [24, 25], optoelectronics [26], and photovoltaics [27]. We note that these reported 2D In_2Se_3 materials have small domain sizes (from a few to tens of micrometers, Figure 1(a) and Table S1) [28–30]. Therefore, controllable growth of high quality 2D In_2Se_3 with large domains is of great importance to further advance the use of 2D In_2Se_3.

To grow 2D materials with large domains, the control of nucleation density is critical, as has been extensively studied in graphene growth [31]. Usually, in the vapor deposition process, the gas flow is controlled to be viscous laminar in order to obtain a constant atmosphere [32]. As shown in Figure S2a, there is a velocity gradient of gas in a reactor, and the velocity gradually decreases to zero near the substrate surface, forming a stagnant layer above the substrate. Due to the fact that the precursor concentration on the substrate surface can influence the nucleation density, controlling the precursor concentration on the surface is important to control the nucleation of the 2D materials (Figure S2b). By analyzing the vapor phase deposition process, we have obtained the following formula for the precursor concentration on the surface (C_s):

$$C_s \sim \frac{1}{1 + k_s/\sqrt{d}} C_g \tag{1}$$

where C_g is the precursor concentration in the gas phase, k_s is the surface reaction rate, and d is the characteristic size of the growth reactor (Table S2). Based on formula (1), C_s decreases as d decreases, causing a lower concentration of precursor on the surface and consequently there is a lower nucleation density of 2D materials in a smaller growth reactor.

Based on the above analyses and previous works [33, 34], we designed a confined micro-reactor to greatly reduce the size of the growth space so as to grow 2D In_2Se_3 with large domain sizes. Specifically, the micro-reactor is composed of two slices of mica with a face-to-face stacking feature. First, the size of growth space is effectively reduced by two to three orders, from 10^5-10^4 μm to 10^2 μm, so that the nucleation density of 2D In_2Se_3 is reduced. Second, the mica, used as a substrate for van der Waals epitaxial growth, benefits the growth of 2D In_2Se_3 with large domain sizes and thin thickness, because the atomically smooth surface and lack of dangling bonds greatly reduce strain from lattice mismatch between the mica and In_2Se_3. As a result, in the confined micro-reactor, high-quality In_2Se_3 with domain sizes larger than 200 μm has been grown on the mica. Moreover, direct growth on flexible mica facilitates the fabrication of flexible photodetectors which have a response time of 140 ms for rise and 25 ms for decay, high responsivity (5.6 A/W), high detectivity (7×10^{10} Jones), and large external quantum efficiency (EQE, 251%). After bending 1000 times, the photodetector showed a steady photocurrent with an 80% retention, indicating good flexibility.

2. Results

As shown in Figure 1(b), the confined micro-reactor is composed of two slices of freshly cleaved mica, stacked face to face. The space (d) between them is only 140 μm, as seen from a side-view scanning electron microscope (SEM) image (inset of Figure 1(b)). This is two to three orders of magnitude smaller than the diameter of the quartz tube in conventional growth experiments (~20-50 mm). To grow the In_2Se_3, In_2Se_3 powder was used as the precursor, and the two slices of mica served as a micro-reactor (see details in Supplementary Materials and Figure S3). Because of the design of this reactor (Figure 1(c)), we obtained 2D In_2Se_3 with large domain sizes. As shown in Figure 1(e), the products are triangular with sharp edges and large domain sizes. In contrast, in In_2Se_3 grown in a conventional reactor (d > 20 mm, Figure 1(d)), the surface of mica is dirtier and the In_2Se_3 crystals grown have smaller domain sizes as shown in Figure 1(f). Moreover, the edge length and thickness of In_2Se_3 samples grown in two different reactors were measured by atomic force microscopy (AFM, Figures 1(g), 1(h), and S4). The results show that the average edge length and thickness of In_2Se_3 are 110 μm and 3.6 nm, respectively, grown in the space-confined micro-reactor. This average edge length of 110 μm is much larger than that of In_2Se_3 grown in the conventional substrate, with an average edge length of 40 μm (Figure 1(g)).

Insight into the structure and chemical composition of the In_2Se_3 was obtained from spectroscopic characterization. Figure 2(a) shows Raman spectra of the In_2Se_3 collected at different positions using a 532 nm excitation laser. All spectra show three typical peaks at ~108, 180, and 203 cm^{-1}, corresponding to the A_1(LO+TO), A_1(TO), and A_1(LO) phonon modes of In_2Se_3, respectively. We compared the Raman spectra with those of 2D exfoliated In_2Se_3 by using a scotch tape (pink curve, Figure 2(a)) and data from recent literature [25], and they all match well. To confirm the uniformity of the In_2Se_3, we also performed Raman mapping (Figure 2(b)), which indicated good uniformity and homogeneity of the material grown in the confined micro-reactor. The X-ray photoelectron spectroscopy (XPS) spectrum of In 3d shows two peaks located at 452.20 and 444.80 eV from In $3d_{3/2}$ and In $3d_{5/2}$, originating from In_2Se_3 (Figure 2(c)). Similarly, the XPS spectrum of Se 3d shows two peaks at 54.80 and 53.80 eV from Se $3d_{3/2}$ and Se $3d_{5/2}$, also attributed to In_2Se_3 (Figure 2(d)) [35]. In addition, the XPS results show that the In_2Se_3 has good stoichiometry with an In/Se atomic ratio close to 2:3 (Figure S5). Ultraviolet-visible-near infrared absorption spectroscopy (UV-Vis-NIR) was used to study the optical bandgap of the In_2Se_3 (Figure 2(e)) which is obtained from the following equation:

$$(\alpha E)^{1/n} = C\left(E - E_g\right) \tag{2}$$

where α is the effective absorption coefficient of the material, E is incident photon energy, C is a constant, E_g is the optical bandgap of the material, and n denotes the nature of

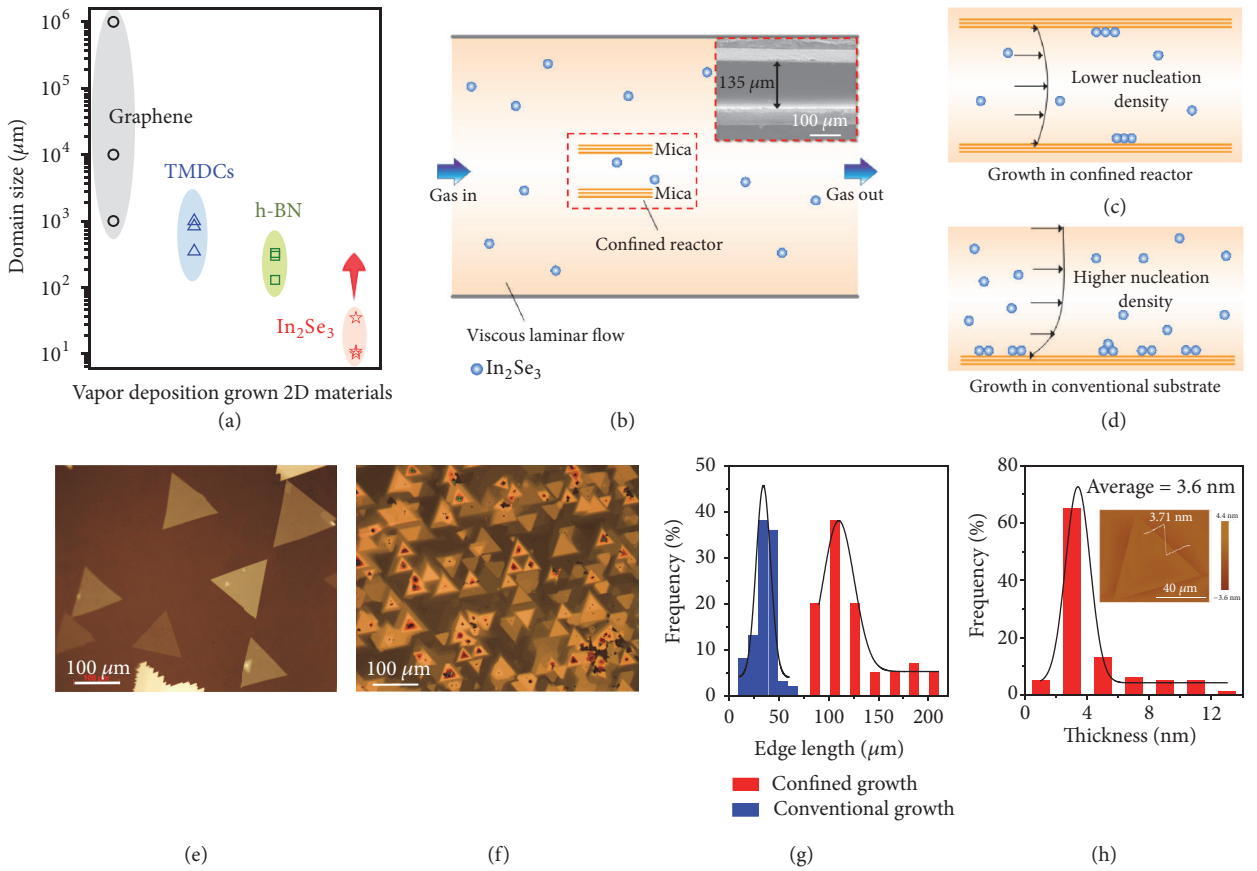

FIGURE 1: Growth of 2D In_2Se_3 with large domain sizes in a confined micro-reactor. (a) A summary of the domain sizes of 2D materials including graphene, TMDCs, h-BN, and In_2Se_3 grown by conventional vapor phase deposition. (b) Schematic of the confined micro-reactor for the growth of 2D In_2Se_3 on mica with large domain sizes. The inset shows a side-view SEM image of the reactor, which is composed of two stacked mica sheets with an average distance of 135 μm between them. (c, d) Schematics showing different gas flow behaviors in the (c) confined and (d) conventional growth methods. (e, f) Optical images of In_2Se_3 crystals grown on the mica substrates with confined and conventional growth. (g, h) Statistical data of the edge length and thickness of In_2Se_3 grown using the two methods. The inset in (h) shows a typical AFM image of 2D In_2Se_3 grown in the confined micro-reactor.

the sample transition, which equals 2 for indirect bandgap materials and 0.5 for direct bandgap materials. E_g was calculated to be 1.48 eV for n = 0.5 (Figure 2(f)), which is close to the value reported in previous work (1.36 eV) [20]. In total, all these spectroscopy results indicate that the synthesized materials are uniform In_2Se_3 with good stoichiometry and optical quality.

We also investigated the structure and crystal quality of the material using X-ray diffraction (XRD) and transmission electron microscopy (TEM). The XRD pattern of the In_2Se_3 grown on the mica substrate in the confined reactor was compared with the patterns of bulk In_2Se_3 and mica, and it was found that, except for the peaks from the mica substrate, all peaks originated from In_2Se_3 (Figure S6). Additionally, the In_2Se_3 has a high crystallinity because the peaks are very sharp. The TEM samples were prepared using a modified transfer method assisted by polydimethylsiloxane (PDMS) and polymethyl methacrylate (PMMA, see details in the Supporting Information). After repeated trial and error, we developed this method to transfer 2D In_2Se_3 onto arbitrary substrates such as plastics, SiO_2/Si, a copper grid, and indium tin oxide (ITO) glass (Figures S7a-d). Raman spectra show that the transferred samples have very similar spectra to the as-grown ones (Figures S7e-i), indicating that negligible damage was done to the samples during transfer. Figure 3(a) shows a high-angle annular dark-field scanning TEM (HAADF-STEM) image of a triangular 2D In_2Se_3 flake. The corresponding energy dispersive X-ray spectroscopy (EDS) elemental maps show the uniform distributions of In and Se atoms in the In_2Se_3 (Figures 3(b) and 3(c)). In addition, quantitative analysis of the EDS results (Figure 3(d)) shows an In:Se atomic ratio of 2:3, in good agreement with the XPS results. Figure 3(e) is an optical image of a In_2Se_3 flake transferred onto a TEM copper grid. The high-resolution TEM (HRTEM) image confirms that it has high quality, and the lattice spacing of 0.35 nm corresponds to the In_2Se_3 (100) lattice planes (Figure 3(f)) [40]. Selected area electron diffraction (SAED, Figures 3(g)–3(l)) patterns were recorded from six positions in this flake (marked 1–6 in Figure 3(e)) far away from each other. It can be seen that all the patterns

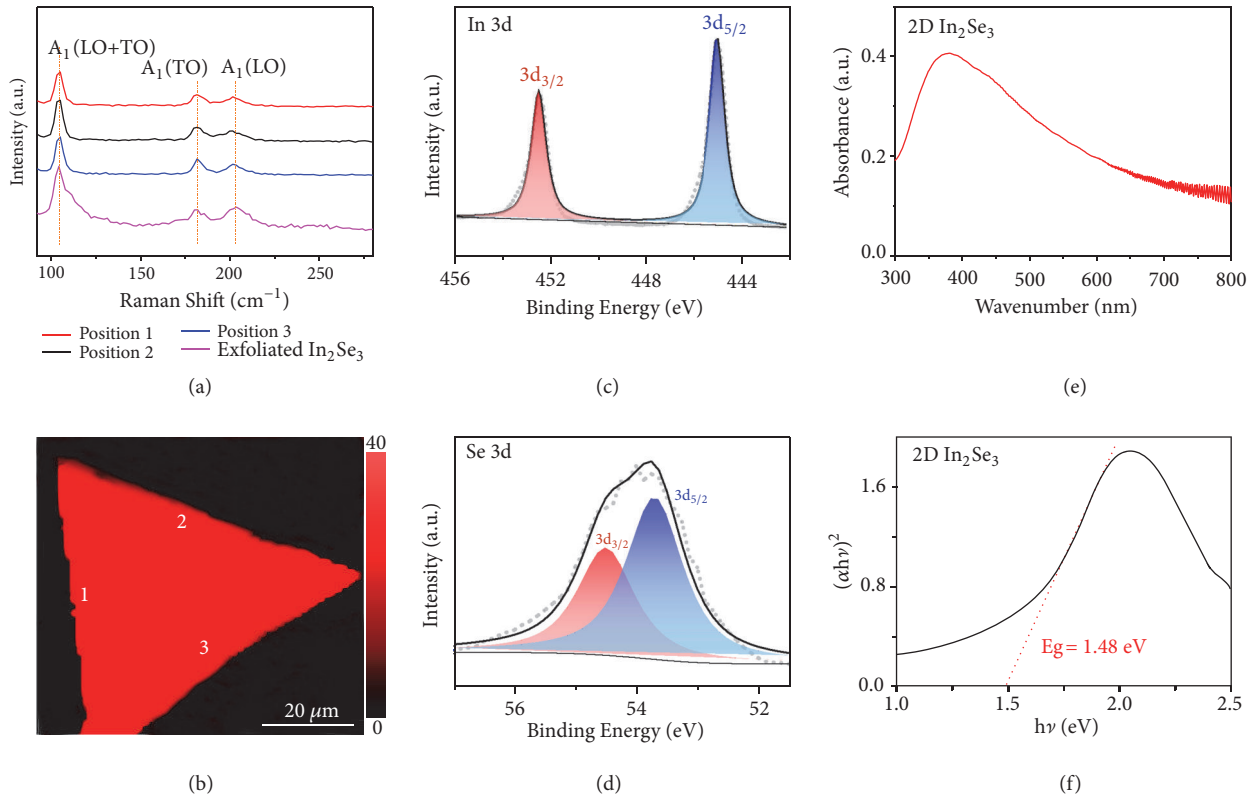

FIGURE 2: Spectroscopic characterization of the as-grown 2D In_2Se_3 in the confined micro-reactor. (a) Raman spectra of In_2Se_3. The three typical Raman peaks at ~108, ~180, and ~203 cm^{-1} are attributed to the A_1(LO+TO), A_1(TO), and A_1(LO) phonon modes of In_2Se_3. (b) Raman intensity map of a 2D In_2Se_3 flake with a thickness of ~10 nm, showing good uniformity. (c, d) XPS spectra of the In 3d and Se 3d in In_2Se_3. (e) UV-Vis-NIR absorption spectrum of the In_2Se_3 grown on mica. (f) hν versus $(\alpha h\nu)^2$ plot of the sample.

have hexagonal symmetry with the same crystallographic orientation, confirming that it is a single crystal domain. All these results confirm that the 2D In_2Se_3 grown in the confined micro-reactor is high quality and highly crystalline.

Generally, compared to monolayer semiconductors, few-layer ones with direct and appropriate bandgaps are promising candidates for photodetectors due to their enhanced light absorption, lower energy loss during photo-electron conversion, and better carrier transfer between source and drain [41]. TMDCs like MoS_2 cannot satisfy all the requirements at the same time because it has an indirect-to-direct bandgap transition when the number of layers decreases from a few layers to a monolayer, so that few-layer MoS_2 has a low photo-electron conversion efficiency and monolayer MoS_2 has weak light absorption.[39, 42] Hence, for MoS_2 and many other TMDCs, a sacrifice of properties is unavoidable to get a balance between light absorption and photo-electron conversion efficiency [43]. Fortunately, In_2Se_3 is a direct bandgap material regardless of its thickness and shows clear advantages in optoelectronics [22, 23]. Therefore, we fabricated two terminal devices on a flexible mica substrate using 2D In_2Se_3 with large domain sizes and high quality as the channel material and studied their photoresponse behavior (Figures 4(a) and 4(b)). Several key parameters including dark current (I_{dark}), rise time (t_r), decay time (t_d), responsivity (R), detectivity (D^*), and EQE were systematically investigated under 660 nm incident light. Figure 4(c) shows that the photocurrent (I_{ph} defined as $I_{ph} = I_{light} - I_{dark}$) increases with the incident light power, and the largest on/off ratio reaches 460. Unlike other narrow bandgap semiconductors, In_2Se_3 shows a large photo-induced on-off ratio, due to its appropriate bandgap and high quality, i.e., lack of defects. In order to investigate the response speed and stability of the photodetector, time-resolved photoresponse measurements were performed by turning on/off the incident light with a chopper, while a high-speed oscilloscope was used to monitor the device current. As shown in Figure 4(d), the In_2Se_3 photodetector remains stable under several on/off light switching events (660 nm incident light at $V_{ds} = 1$ V) with a nearly constant "on-state" current of ~25 nA (Figure 4(d)), with t_r and t_d calculated to 140 ms and 25 ms, respectively (Figures 4(e) and 4(f)). We note that the response time is much slower than commercial Si based photodetectors (~5.9 μs). Further engineering and optimization of the quality of materials and interface cleanness of devices should improve the response time. Note that, after bending 1000 times, the current remains steady with a retention of >80% (with an "on-state" current of ~ 20 nA, Figure 4(d)). We also shined 850 and 940 nm incident light on the device and it showed good stability (Figures S8a and S8b). It is well known that

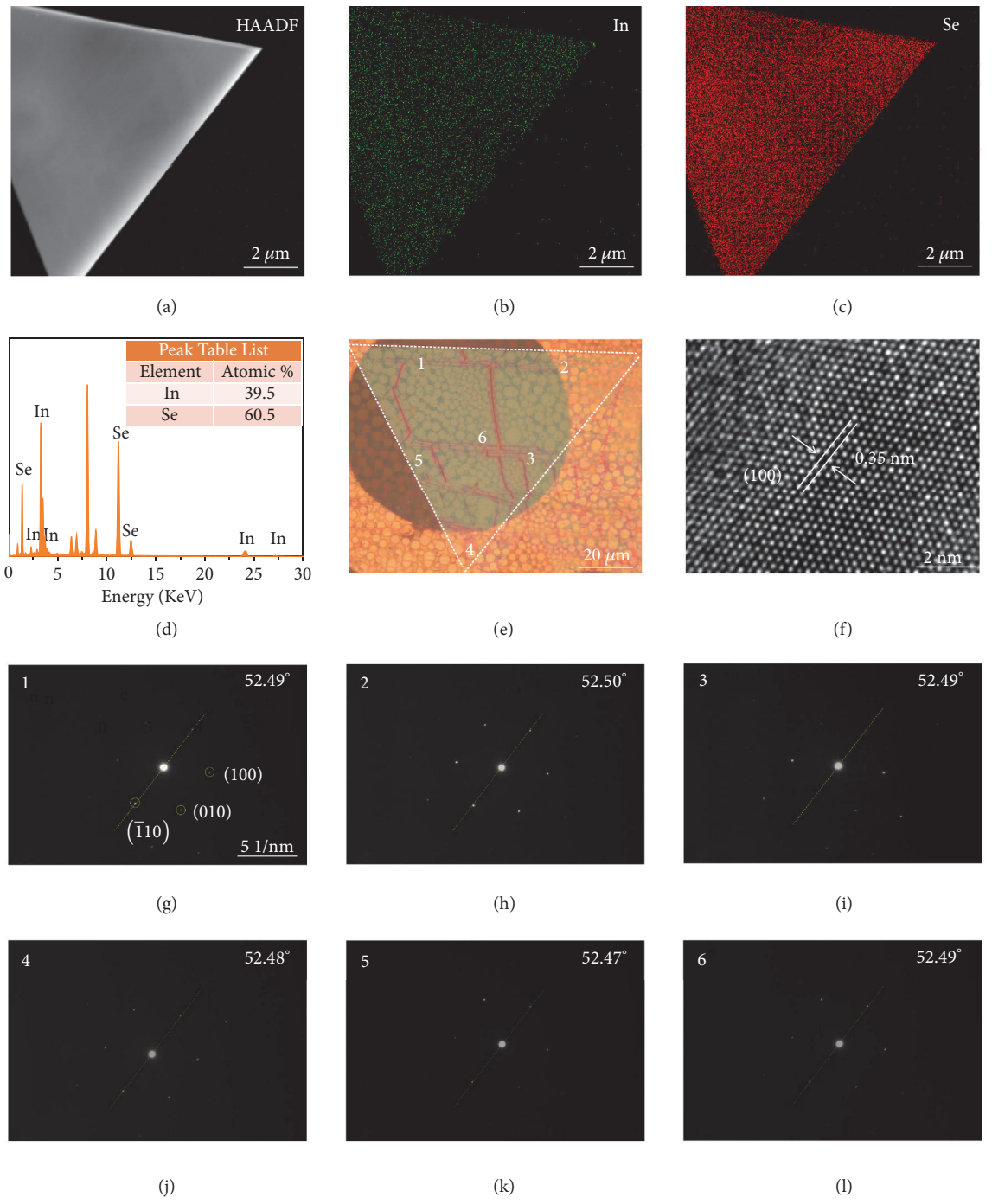

FIGURE 3: Microstructural characterization of the In_2Se_3. (a) HAADF image of In_2Se_3 flake transferred onto a TEM grid. (b, c) EDS maps of In and Se for this In_2Se_3 flake. (d) An EDS spectrum of the sample, which shows an atomic ratio of 2:3 (In:Se). (e, f) Optical microscope (e) and HRTEM (f) images of a In_2Se_3 flake transferred onto a TEM grid. (g–l) SEAD patterns obtained from the six positions labeled 1–6 on the transferred sample in (e).

most semiconductors are sensitive to visible light, but few show an appropriate responsivity and response speed to NIR light. These results suggest that the In_2Se_3 is a promising candidate for high-performance photodetectors in the UV-Vis-NIR region. Meanwhile, when we changed the power of the incident 660 nm light (P_{in}), different I_{ph} values were obtained (Figure S9). The relationship between I_{ph} and P_{in} is fitted by $I_{ph} = aP^{\alpha}$. In our experiments, the parameters a and α were calculated to be 0.89 and 0.68, respectively (Figure 4(g)). Moreover, as shown in Figure 4(h), we obtained

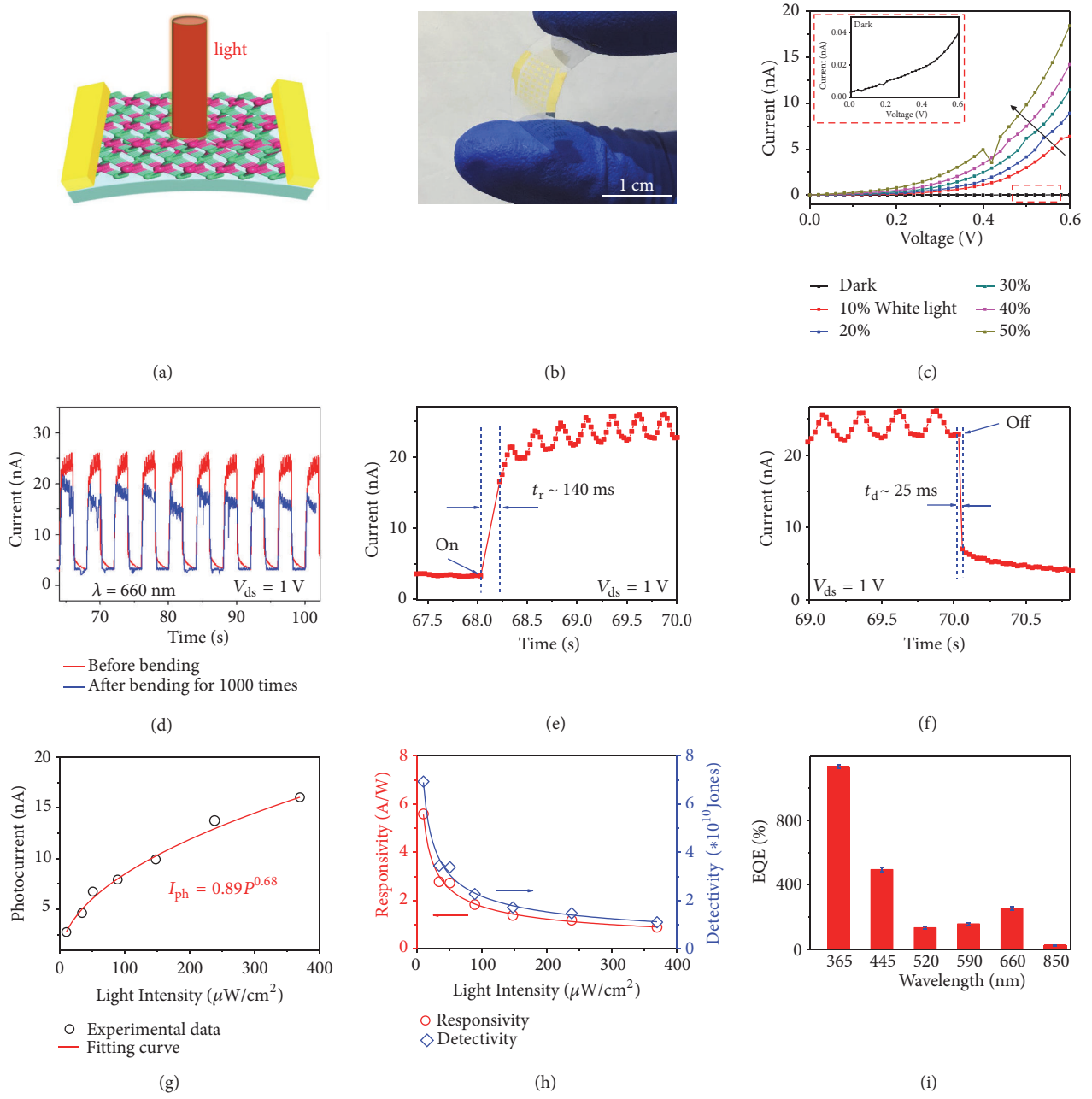

FIGURE 4: 2D In_2Se_3 based flexible photodetectors. (a) Schematic of a flexible photodetector on a mica substrate using a 2D In_2Se_3 flake with a thickness of ~7 nm as the channel material. (b) Photo showing the bendable device of the 2D In_2Se_3 on a mica substrate. (c) Current under white light with different power intensities. (d) Time-resolved photoresponse of the same device with 660 nm light before and after bending 1000 times. (e, f) The exponential curves of the rise and decay times. (g) Photocurrent versus power intensity for 660 nm incident light. (h) Responsivity and detectivity of the device under 660 nm incident light with different powder intensities. (i) The relationship between EQE and different incident light wavelengths (UV-Vis-NIR range). All data were measured at 300 K, under atmospheric conditions and V_{ds} = 1 V.

a remarkable responsivity of 5.6 A/W (under P = 10.2 μW cm^{-2}, V_{ds} = 1 V), which was calculated from the following formula:

$$R = \frac{I_{ph}}{P_{in}S} \tag{3}$$

where R is the responsivity and S is the effective area of the photodetector. This responsivity is 10^3 times higher than the reported value of multilayer MoS_2-based phototransistors (around 7.5×10^{-3} A/W), presumably because few-layer MoS_2 has an indirect bandgap [37]. In addition, based on the following formula,

Table 1: A comparison of the photoresponse of In_2Se_3 with other 2D materials.

Materials	Responsivity (A/W)	Rise time (ms)	Decay time (ms)	Spectral range	Type	Ref.
Graphene (on SiO_2/Si)	1×10^{-3}	10^{-6}	NA	Visible	Rigid	[36]
MoS_2 (on SiO_2/Si)	7.5×10^{-3}	50	50	Visible	Rigid	[37]
BP (on SiO_2/Si)	4.8×10^{-3}	1	NA	Visible-NIR	Rigid	[38]
In_2Se_3 (on SiO_2/Si)	2.5	NA	NA	Visible	Rigid	[28]
WSe_2 (on PI)	0.92	900	2000	UV-NIR	Flexible	[39]
In_2Se_3 (on mica)	5.6	140	25	UV-NIR	Flexible	This work

$$D^* = \frac{RS^{1/2}}{(2eI_{dark})^{1/2}} \quad (4)$$

where D^* is detectivity and e is the charge of an electron, we calculated the detectivity and found an identical trend with responsivity. Impressively, its maximum D^* reaches 7 $\times 10^{10}$ Jones (under $P = 10.2$ μW cm^{-2}, $V_{ds} = 1$ V) as shown in Figure 4(h), and this value is three orders of magnitude higher than that of MoS_2 photodetectors [37]. This detectivity is superior to the vast majority of reported 2D material-based phototransistors. Finally, we calculated EQE based on the different light photoresponses (Figure S10), using the following:

$$\text{EQE} = \frac{Rhc}{(e\lambda)} \quad (5)$$

where h is Planck's constant, c the velocity of light, and λ the wavelength of the incident light. The EQE of the In_2Se_3 photodetector ($V_{ds} = 1$ V) was calculated to be 1135% at 365 nm, 495% at 445 nm, 127% at 520 nm, 154% at 590 nm, 251% at 660 nm, and 18% at 850 nm. These results suggest that few-layer In_2Se_3 grown on mica, as a direct bandgap semiconductor, is suitable for use in flexible broadband photodetectors.

A comparison of the performance of photodetectors using our 2D In_2Se_3 and other 2D materials is shown in Table 1. Overall, the combination of high responsivity, high detectivity, and flexibility makes In_2Se_3 a promising material for flexible broadband photodetectors. We believe that the large size, high quality, and thin thickness of the In_2Se_3 can prolong the photo-excited carrier lifetime and result in a high photoresponsivity. In addition, the use of a mica substrate which has an atomically flat surface may reduce trap states at the interface between the In_2Se_3 and the mica substrate, leading to long photo-excited carrier lifetime. As shown from the formula $R \propto I_{ph} \propto \Delta\sigma = q(\mu_n + \mu_p)(\Delta p)_0 \exp(-t/\tau)$, it is clear that a longer photo-excited carrier lifetime (τ) leads to improved photoconductivity (σ), a larger photocurrent, and better responsivity.

3. Discussion

In summary, we designed a confined micro-reactor that greatly reduces the size of the growth space and thus the nucleation density of 2D materials. As a result, we achieved the growth of 2D In_2Se_3 with large domain sizes and high quality. Because of the large domain size, high quality, and layer-independent direct bandgap, we have been able to fabricate In_2Se_3-based flexible photodetectors, which have a fast response speed, and high responsivity, detectivity, and EQE. The strategy used here could potentially shed light on the growth of other 2D materials, facilitating their application in a wide-range of devices.

4. Materials and Methods

Materials and Chemicals. In_2Se_3 powder (99.99%, Alfa Aesar, USA), fluorphlogopite mica ($[KMg_3(AlSi_3O_{10})F_2]$, Tiancheng Fluorphlogopite Mica Co., Ltd., China), polydimethylsiloxane (PDMS) tape (200 μm thickness, Hangzhou Bao Er De New Materials Technology Co., Ltd., China), polymethyl methacrylate (PMMA, 950 K, ALLRESIST, AR-P 672.045, Germany), acetone, and ethanol (AR, Shanghai Macklin Biochemical Co., Ltd., China) were used as received.

Vapor Phase Growth of 2D In_2Se_3. In our experiments, growth was conducted in a homemade atmospheric pressure vapor deposition furnace equipped with a 1-inch diameter quartz tube (TF55035C-1, Lindberg/Blue M). The quartz boat containing In_2Se_3 powder was put at the center of the furnace, and two slices of freshly cleaved mica were placed downstream (8-10 cm), stacked face-to-face, and served as a confined micro-reactor for 2D In_2Se_3 growth. The furnace was heated to the growth temperature of 850°C, which was determined by the thermo-gravimetric analysis (Figure S3), with a ramp rate of 30°C min^{-1}, and kept there for 5-30 min for the growth. Ar was introduced during the ramping and growth periods at a flow rate of 50-100 standard cubic centimeters per minute (sccm, with a purity of 99.99%). After growth, the furnace was cooled to room temperature under 50 sccm Ar. In the controlled growth experiments, 2D In_2Se_3 was grown on a freshly cleaved mica substrate placed in the same location but without the other mica sheet.

Transfer of As-Grown 2D In_2Se_3 onto a TEM Grid. The TEM samples were prepared by transferring 2D In_2Se_3 using a PMMA and PDMS assisted transfer method [44]. First, PMMA solution was spin-coated onto the mica substrate with the grown In_2Se_3 (3000 rpm for 1 min). Second, the substrate was heated in air at 170°C for 5 min to form a PMMA film which served as a supporting layer and protected the In_2Se_3 in the following steps. Third, the PDMS tape was placed on the PMMA and the substrate was heated at 180°C

for 5 min to make a strong bond between the PDMS and PMMA. Fourth, the PDMS/PMMA/In_2Se_3 was peeled off the mica substrate. Due to the hydrophobicity of PMMA and hydrophilicity of the mica, some water was introduced at the PMMA/mica interface to assist the separation of PMMA/In_2Se_3 and the mica substrate during the peeling-off. Fifth, the PDMS/PMMA/In_2Se_3 was attached to target substrates, followed by removing the PDMS tape. Finally, the PMMA was removed by hot acetone and the transferred In_2Se_3 sample was dried naturally in an ambient environment for further characterization.

Characterization of 2D In_2Se_3. The side view of the space between the two mica sheets was checked by SEM (Hitachi SU8010, Japan). Optical images of the In_2Se_3 crystal were taken using an optical microscope (Carl Zeiss Microscopy, Germany). The thickness of the In_2Se_3 was determined by AFM (tapping mode, Bruker Dimension Icon, Germany). Raman spectroscopy was performed under a 532 nm laser excitation (Horiba LabRAB HR800, Japan). The laser spot was 1 μm and the laser power on the sample surface was less than ~100 μW. Structural and chemical analyses of the samples were performed by XRD (Cu Kα radiation, λ = 0.15418 nm, Bruker D8 Advance, Germany), XPS (Thermo Scientific K-Alpha XPS, using Al (Kα) radiation as a probe, USA), and TEM (FEI Tacnai F30, 300 kV acceleration voltage, USA) with an attached EDS unit. UV-Vis-NIR absorption was conducted to study the continuous In_2Se_3 films (Perkin-Elmer Lambda 950 spectrophotometer, USA).

Device Fabrication and Measurements. The as-grown In_2Se_3 sample was aligned with a shadow mask and titanium/gold (Ti/Au, 5 nm/50 nm) electrodes were then made by electron beam evaporation. Electrical measurements were conducted under a microprobe station and semiconductor property analyzer (Keithley 4200 SCS, USA) under ambient environment at room temperature. LEDs with different wavelengths ranging from 365 nm to 940 nm were used as incident light during photodetection measurements (CEL-LED535, LED Multiband and High-power Supply, China).

Conflicts of Interest

The authors declare no conflicts of interest.

Authors' Contributions

Lei Tang and Changjiu Teng contributed equally to this work.

Acknowledgments

This work was financially supported by the National Natural Science Foundation of China (Nos. 51521091 and 51722206), the Youth 1000-Talent Program of China, the National Key R&D Program (2018YFA0307200), the Shenzhen Basic Research Project (Nos. JCYJ20170307140956657, JCYJ20160613160524999, JCYJ20170412152620376, and ZDSYS20170303165926217), Trade and Information Commission of Shenzhen Municipality for the "2017 Graphene Manufacturing Innovation Center Project" (No. 201901171523), Guangdong Innovative and Entrepreneurial Research Team Program (Grant No. 2017ZT07C341), and the Development and Reform Commission of Shenzhen Municipality for the development of the "Low-Dimensional Materials and Devices" discipline.

Supplementary Materials

Figure S1. Crystal structure of layered In_2Se_3 with each layer composed of Se-In-Se-In-Se atomic sheets. *Figure S2*. Schematics showing viscous laminar flow in the vapor deposition process and related physical parameters. *Figure S3*. Thermo-gravimetric analysis of the In_2Se_3 source in an Ar atmosphere, and the temperature window for the growth of 2D In_2Se_3 in this work is shown by the green region. *Figure S4*. AFM images of the as-grown 2D In_2Se_3 on mica by confined growth. *Figure S5*. Survey XPS spectrum of as-grown 2D In_2Se_3 on mica. *Figure S6*. XRD patterns of 2D In_2Se_3 grown on mica (red) with reference patterns from a blank mica substrate (blue), bulk In_2Se_3 (green), and a simulated diffractogram (black). *Figure S7*. PDMS assisted transfer of 2D In_2Se_3 from a mica substrate onto different substrates. *Figure S8*. Time-resolved photoresponse of the 2D In_2Se_3 photodetector under 850 nm and 940 nm light. *Figure S9*. I–V curves of the 2D In_2Se_3 photodetector under 660 nm incident light with different power values. *Figure S10*. I–V curves of the 2D In_2Se_3 photodetector under different incident light wavelengths. *(Supplementary Materials)*

References

[1] Z. Cai, B. Liu, X. Zou, and H.-M. Cheng, "Chemical vapor deposition growth and applications of two-dimensional materials and their heterostructures," *Chemical Reviews*, vol. 118, no. 13, pp. 6091–6133, 2018.

[2] M. Huang, M. Biswal, H. J. Park et al., "Highly oriented monolayer graphene grown on a Cu/Ni(111) alloy foil," *ACS Nano*, vol. 12, no. 6, pp. 6117–6127, 2018.

[3] Y. Liu and B. I. Yakobson, "Cones, pringles, and grain boundary landscapes in graphene topology," *Nano Letters*, vol. 10, no. 6, pp. 2178–2183, 2010.

[4] X. Cai, Y. Luo, B. Liu, and H.-M. Cheng, "Preparation of 2D material dispersions and their applications," *Chemical Society Review*, vol. 47, pp. 6224–6266, 2018.

[5] L. Peng, Z. Xu, Z. Liu, Y. Guo, P. Li, and C. Gao, "Ultrahigh thermal conductive yet superflexible graphene films," *Advanced Materials*, vol. 29, no. 27, pp. 1700589–1700596, 2017.

[6] X. Zhang, T. H. Choudhury, M. Chubarov et al., "Diffusion-controlled epitaxy of large area coalesced WSe_2 monolayers on sapphire," *Nano Letters*, vol. 18, no. 2, pp. 1049–1056, 2018.

[7] J. Wu, H. Yuan, M. Meng et al., "High electron mobility and quantum oscillations in non-encapsulated ultrathin semiconducting Bi_2O_2Se," *Nature Nanotechnology*, vol. 12, no. 6, pp. 530–534, 2017.

[8] J. Li, Z. X. Wang, Y. Wen et al., "High-performance near-infrared photodetector based on ultrathin Bi_2O_2Se nanosheets," *Advanced Functional Materials*, vol. 28, no. 10, p. 1706437, 2018.

[9] T. Wu, X. Zhang, Q. Yuan et al., "Fast growth of inch-sized single-crystalline graphene from a controlled single nucleus on Cu-Ni alloys," *Nature Materials*, vol. 15, no. 1, pp. 43–47, 2016.

[10] I. V. Vlassiouk, Y. Stehle, P. R. Pudasaini et al., "Evolutionary selection growth of two-dimensional materials on polycrystalline substrates," *Nature Materials*, vol. 17, no. 4, pp. 318–322, 2018.

[11] M. Wang, J. Wu, L. Lin et al., "Chemically engineered substrates for patternable growth of two-dimensional chalcogenide crystals," *ACS Nano*, vol. 10, no. 11, pp. 10317–10323, 2016.

[12] L. Gao, W. Ren, H. Xu et al., "Repeated growth and bubbling transfer of graphene with millimetre-size single-crystal grains using platinum," *Nature Communications*, vol. 3, pp. 699–705, 2012.

[13] X. Xu, Z. Zhang, J. Dong et al., "Ultrafast epitaxial growth of metre-sized single-crystal graphene on industrial Cu foil," *Chinese Science Bulletin*, vol. 62, no. 15, pp. 1074–1080, 2017.

[14] W. Chen, J. Zhao, J. Zhang et al., "Oxygen-assisted chemical vapor deposition growth of large single-crystal and high-quality monolayer MoS_2," *Journal of the American Chemical Society*, vol. 137, no. 50, pp. 15632–15635, 2015.

[15] Y. Gao, Y. L. Hong, L. C. Yin et al., "Ultrafast growth of high-quality monolayer WSe_2 on Au," *Advanced Materials*, vol. 29, no. 29, pp. 1700990–1700997, 2017.

[16] T. Yang, B. Zheng, Z. Wang et al., "Van der Waals epitaxial growth and optoelectronics of large-scale WSe_2/SnS_2 vertical bilayer p-n junctions," *Nature Communications*, vol. 8, no. 1, pp. 1906–1914, 2017.

[17] Y. Ji, B. Calderon, Y. Han et al., "Chemical vapor deposition growth of large single-crystal Mono-, Bi-, Tri-layer hexagonal boron nitride and their interlayer stacking," *ACS Nano*, vol. 11, no. 12, pp. 12057–12066, 2017.

[18] L. Wang, B. Wu, H. Liu et al., "Water-assisted growth of large-sized single crystal hexagonal boron nitride grains," *Materials Chemistry Frontiers*, vol. 1, no. 9, pp. 1836–1840, 2017.

[19] G. Lu, T. Wu, Q. Yuan et al., "Synthesis of large single-crystal hexagonal boron nitride grains on Cu-Ni alloy," *Nature Communications*, vol. 6, pp. 6160–6166, 2015.

[20] W. Feng, W. Zheng, F. Gao et al., "Sensitive electronic-skin strain sensor array based on the patterned two-dimensional α-In_2Se_3," *Chemistry of Materials*, vol. 28, no. 12, pp. 4278–4283, 2016.

[21] B. Sirota, N. Glavin, S. Krylyuk, A. V. Davydov, and A. A. Voevodin, "Hexagonal $MoTe_2$ with amorphous BN passivation layer for improved oxidation resistance and endurance of 2D field effect transistors," *Scientific Reports*, vol. 8, no. 1, pp. 8668–8675, 2018.

[22] W. Ding, J. Zhu, Z. Wang et al., "Prediction of intrinsic two-dimensional ferroelectrics in In_2Se_3 and other III2-VI3 van der Waals materials," *Nature Communications*, vol. 8, pp. 14956–14963, 2017.

[23] Z. Q. Zheng, J. D. Yao, and G. W. Yang, "Growth of centimeter-scale high-quality In_2Se_3 films for transparent, flexible and high performance photodetectors," *Journal of Materials Chemistry C*, vol. 4, no. 34, pp. 8094–8103, 2016.

[24] F. Xue, J. Zhang, W. Hu et al., "Multidirection piezoelectricity in mono- and multilayered hexagonal α-In_2Se_3," *ACS Nano*, vol. 12, no. 5, pp. 4976–4983, 2018.

[25] Y. Zhou, D. Wu, Y. Zhu et al., "Out-of-plane piezoelectricity and ferroelectricity in layered α-In_2Se_3 nanoflakes," *Nano Letters*, vol. 17, no. 9, pp. 5508–5513, 2017.

[26] T. Zhai, X. Fang, M. Liao et al., "Fabrication of high-quality In_2Se_3 nanowire arrays toward high-performance visible-light photodetectors," *ACS Nano*, vol. 4, no. 3, pp. 1596–1602, 2010.

[27] I. Bouchama, S. Boudour, N. Bouarissa, and Z. Rouabah, "Quantum and conversion efficiencies optimization of superstrate CIGS thin-films solar cells using In_2Se_3 buffer layer," *Optical Materials*, vol. 72, pp. 177–182, 2017.

[28] M. Lin, D. Wu, Y. Zhou et al., "Controlled growth of atomically thin In_2Se_3 flakes by van der Waals epitaxy," *Journal of the American Chemical Society*, vol. 135, no. 36, pp. 13274–13277, 2013.

[29] J. Zhou, Q. Zeng, D. Lv et al., "Controlled synthesis of high-quality monolayered α-In_2Se_3 via physical vapor deposition," *Nano Letters*, vol. 15, no. 10, pp. 6400–6405, 2015.

[30] W. Zheng, T. Xie, Y. Zhou et al., "Patterning two-dimensional chalcogenide crystals of Bi_2Se_3 and In_2Se_3 and efficient photodetectors," *Nature Communications*, vol. 6, no. 1, pp. 6972–6979, 2015.

[31] H. Wang, X. Xu, J. Li et al., "Surface monocrystallization of copper foil for fast growth of large single-crystal graphene under free molecular flow," *Advanced Materials*, vol. 28, no. 40, pp. 8968–8974, 2016.

[32] S. Bhaviripudi, X. Jia, M. S. Dresselhaus, and J. Kong, "Role of kinetic factors in chemical vapor deposition synthesis of uniform large area graphene using copper catalyst," *Nano Letters*, vol. 10, no. 10, pp. 4128–4133, 2010.

[33] X. Wang, Y. Gong, G. Shi et al., "Chemical vapor deposition growth of crystalline monolayer $MoSe_2$," *ACS Nano*, vol. 8, no. 5, pp. 5125–5131, 2014.

[34] C. Cong, J. Shang, X. Wu et al., "Synthesis and optical properties of large-area single-crystalline 2D semiconductor WS_2 monolayer from chemical vapor deposition," *Advanced Optical Materials*, vol. 2, no. 2, pp. 131–136, 2014.

[35] A. J. Nelson, A. B. Swartzlander, J. R. Tuttle, R. Noufi, R. Patel, and H. Höchst, "Photoemission investigation of the electronic structure at polycrystalline $CuInSe_2$ thin-film interfaces," *Journal of Applied Physics*, vol. 74, no. 9, pp. 5757–5760, 1993.

[36] F. Xia, T. Mueller, Y.-M. Lin, A. Valdes-Garcia, and P. Avouris, "Ultrafast graphene photodetector," *Nature Nanotechnology*, vol. 4, no. 12, pp. 839–843, 2009.

[37] Z. Yin, H. Li, H. Li et al., "Single-layer MoS_2 phototransistors," *ACS Nano*, vol. 6, no. 1, pp. 74–80, 2012.

[38] H. Yuan, X. Liu, F. Afshinmanesh et al., "Polarization-sensitive broadband photodetector using a black phosphorus vertical p-n junction," *Nature Nanotechnology*, vol. 10, no. 8, pp. 707–713, 2015.

[39] Z. Q. Zheng, T. M. Zhang, J. D. Yao, Y. Zhang, J. R. Xu, and G. W. Yang, "Flexible,transparent and ultra-broadband photodetector based on large-area WSe_2 film for wearable devices," *Nanotechnology*, vol. 27, no. 22, pp. 225501–225511, 2016.

[40] R. B. Jacobs-Gedrim, M. Shanmugam, N. Jain et al., "Extraordinary photoresponse in two-dimensional In_2Se_3 nanosheets," *ACS Nano*, vol. 8, no. 1, pp. 514–521, 2014.

[41] D. Lembke, S. Bertolazzi, and A. Kis, "Single-layer MoS_2 electronics," *Accounts of Chemical Research*, vol. 48, no. 1, pp. 100–110, 2015.

[42] Q. Ji, Y. Zhang, T. Gao et al., "Epitaxial monolayer MoS_2 on mica with novel photoluminescence," *Nano Letters*, vol. 13, no. 8, pp. 3870–3877, 2013.

[43] A. Splendiani, L. Sun, Y. Zhang et al., "Emerging photoluminescence in monolayer MoS_2," *Nano Letters*, vol. 10, no. 4, pp. 1271–1275, 2010.

[44] L. Guo, H. Yan, Q. Moore et al., "Elastic properties of van der Waals epitaxy grown bismuth telluride 2D nanosheets," *Nanoscale*, vol. 7, no. 28, pp. 11915–11921, 2015.